

## Article

# Sensorless Control Method for SPMSMs Based on Improved Sliding Mode Reaching Rate

Yuepeng Chen <sup>1</sup>, Aiyi Li <sup>1</sup> , Hui Li <sup>2</sup>, Xu Yang <sup>1,\*</sup> and Wei Chen <sup>3,\*</sup><sup>1</sup> School of Automation, Wuhan University of Technology, Wuhan 430070, China<sup>2</sup> Wuhan Ship Development & Design Institute, Wuhan 430060, China<sup>3</sup> School of Urban Construction, Wuhan University of Science and Technology, Wuhan 430065, China

\* Correspondence: yx\_auto@whut.edu.cn (X.Y.); nancychw@wust.edu.cn (W.C.)

**Abstract:** Due to the advantages of simple structure, small size, and high power density, permanent magnet synchronous motors (PMSM) have attracted the research interest of many scholars both domestically and abroad. However, traditional PMSM equipped with sensors, encoders, and other devices tend to have high equipment costs and rely heavily on the accuracy of the sensors for control effectiveness. Therefore, sensorless control has become a hot trend in the PMSM control field. In response to the chattering problem in sliding mode algorithms, this study first optimized the sliding mode reaching rate of a sensorless control system and applied it to construct a sliding mode observer and speed controller. Next, the improved sliding mode reaching rate-based sensorless control system was modeled and simulated in Matlab/Simulink, and its control performance was compared and analyzed with that of the traditional sliding mode reaching rate and replicated sliding mode reaching rate. Finally, comparative experiments were conducted on a test bench, and the results showed that, under the action of the improved sliding mode reaching rate, the chattering range of the output speed of the motor was +2%~+5%, which optimized the output speed of the PMSM and achieved the purpose of weakening the chattering.

**Keywords:** PMSM; sensorless control; SMO; sliding mode reaching rate; chattering



**Citation:** Chen, Y.; Li, A.; Li, H.; Yang, X.; Chen, W. Sensorless Control Method for SPMSMs Based on Improved Sliding Mode Reaching Rate. *Electronics* **2023**, *12*, 3720. <https://doi.org/10.3390/electronics12173720>

Academic Editor: Ahmed Abu-Siada

Received: 13 June 2023

Revised: 3 August 2023

Accepted: 1 September 2023

Published: 3 September 2023



**Copyright:** © 2023 by the authors. Licensee MDPI, Basel, Switzerland. This article is an open access article distributed under the terms and conditions of the Creative Commons Attribution (CC BY) license (<https://creativecommons.org/licenses/by/4.0/>).

## 1. Introduction

Permanent magnet synchronous motors (PMSMs) are highly favored by engineers because of their compact size, lightweight construction, high power factor, and reliability [1,2]. These motors have wide applications in industrial automation equipment and appliances, as well as high-performance digital and intelligent servo systems used in aerospace applications. The need for effective control of PMSMs is crucial to meet the control requirements of these application scenarios. However, PMSMs are characterized by complexity, multivariable behavior, nonlinearity, and strong coupling from a mathematical modeling perspective. Therefore, it is essential to decouple the system in order to achieve efficient control of PMSMs. Various corresponding control strategies have been proposed, including PI control, vector control, sliding mode control (SMC), model predictive control, adaptive control, and intelligent control [3]. Traditional vector control systems utilize encoders and mechanical sensors to measure the rotor speed and angle position of the motors. However, this approach not only escalates the cost of the control system but also introduces dependency on the reliability of the sensors. Additionally, there may be electromagnetic interference and other adverse effects. Scholars in the field of sensorless control of PMSM have shown significant interest in addressing these engineering problems.

Presently, mainstream sensorless control technologies can be categorized into two groups: high-frequency signal injection and observer-based methods that rely on the motor model. The method of high-frequency signal injection involves injecting a high-frequency voltage signal into the stator power supply. The rotor's position influences

the amplitude of the high-frequency current generated on two distinct reference axes due to the magnetic saliency of the rotor. The estimation of the rotor position becomes possible by accurately demodulating and analyzing the signals generated. However, this method is primarily suitable for the low-speed range, and it can result in several drawbacks, including additional losses, noise, and increased distortion of the total harmonic current. The observer-based method estimates the motor parameters, such as the back electromotive force, in either the stationary or rotating reference frame to determine the rotor position. This method is suitable for a range of medium-to-high speeds. Additionally, several observer algorithms have been proposed and developed, including the state observer (SO) [4], the sliding mode observer (SMO), the disturbance observer (DO), and the full-order observer, among others.

Among various observer algorithms, the approach described in references [5–7] involves utilizing the back electromotive force (EMF) as a disturbance and estimating it through a disturbance observer to achieve sensorless control. This method demonstrates high reliability and rapid response. However, the disturbance observer algorithm necessitates a high level of model accuracy and is sensitive to motor model parameters, which ultimately compromises its robustness. References [8–12] employed an extended state observer to attain sensorless control of PMSM. Nevertheless, the linear state observer-based sensorless control system encounters difficulties in tracking rapidly changing back EMF, and the algorithm itself becomes significantly complicated when addressing delay issues arising from higher-order differentiation. Reference [13] employed an adaptive full-order observer design method. However, the full-order observer necessitates significant computational power for both feedback gain matrix and parameter self-tuning, rendering it unsuitable for practical engineering applications. References [14–20] utilized sliding mode observers to achieve sensorless control. The sliding mode observer is a nonlinear observer grounded in sliding mode control theory, exhibiting robustness against system parameter changes, resistance to disturbances, and adaptability to internal and external interferences. By utilizing control switch signals, it compels the estimated state variable error to approach the designated sliding mode surface, leading to the convergence of the estimated output state variables towards their expected values. Scholars referenced in [14–18] have conducted research on the application of sliding mode observers in sensorless control. They achieved the measurement of rotor speed and angle position by observing the back electromotive force (EMF) and utilizing technologies such as the phase-locked loop (PLL) and the arc-tangent function [21].

The sliding mode observer algorithm possesses notable qualities, including simplicity of implementation, robustness, and efficient real-time performance, all achieved without requiring intricate computations. It serves as an efficient, precise, robust, and real-time control method. However, the use of a discontinuous switching function in the sliding mode algorithm can lead to chattering in the estimation of state variables. In motor control systems, the chattering of the motor output speed and the observer's estimated state reflect the system's performance level. Many researchers have made improvements to the sliding mode algorithm to mitigate the impact of chattering and enhance control system performance. For instance, in [16], an adaptive sliding mode observer was proposed to attenuate chattering; however, its practical application is hindered by the substantial computational requirements. Reference [17] suggested employing the sigmoid function instead of the switching function, but this method utilizes a fixed sliding mode gain. If the gain is set excessively high, the estimated value of the state variable will exhibit chattering. Conversely, if the gain is too small, the convergence time will be compromised. Reference [18] introduced an enhanced full-order sliding mode observer that replaces the switching function with piecewise functions to suppress chattering and improve control performance. Although piecewise functions offer improved smoothness, continuity, and differentiability compared to switching functions, they amplify the complexity of full-order observers and necessitate greater computing resources, potentially resulting in prolonged system response times. Some scholars have proposed new reaching rates based on the sliding mode reach-

ing rate to address chattering optimization concerns. Reference [22] adopted a saturation function to reduce chattering by restricting the output value through the thickness of the saturation function. Nonetheless, this approach may cause the output value to remain constant within the saturation interval, leading to static errors in the system. Reference [23] proposed using fractional integral sliding mode surfaces to alleviate chattering, but the integration term in the algorithm requires intensive computational resources and may accumulate errors. Reference [24] considered the design of a novel sliding mode reaching rate that incorporates exponential terms, terminal terms, system states, and variable terms to enhance control performance. However, disturbances during motor operation can impact the system, and the variable gain in the sliding mode observer fails to effectively adapt to changes. A suitable reaching rate ensures rapid trajectory convergence towards the sliding mode switching surface when the motion point is distant from it [25]. As the sliding mode surface is approached, the convergence rate gradually diminishes towards zero to minimize system chattering. This article proposed an improvement to the reaching rate of the sliding mode control by introducing an error term that adjusts the gain value based on real-time error variations. When the error between the actual and reference speeds is significant, the gain value increases to improve the convergence speed. As the error reduces, the gain value gradually decreases, ensuring convergence quality and facilitating adaptive gain adjustment. Through simulation analysis and experimental verification, this improved algorithm demonstrated favorable outcomes in terms of vibration optimization.

In order to address the issue of chattering in the traditional sliding mode algorithm, this paper proposes a novel sliding mode reaching rate that optimizes the trade-off between system chattering and convergence time, enabling sensorless control of PMSM. Section 1 provides an introduction to the background of the motor control field. Section 2 presents the mathematical model of the PMSM. In Section 3, a contradiction point is identified in the conventional sliding mode reaching law by calculating the convergence time. Subsequently, an enhanced sliding mode reaching law is introduced and the sufficient conditions for convergence are derived using the Lyapunov function. Section 4 proposes an improved SMO and SMC based on the improved sliding mode reaching rate. Additionally, it develops a simulation model for sensorless control of PMSM. In Section 5, a comparative analysis is conducted to compare the performance of the proposed methods through simulations and experimental validations. The results demonstrate that the improved sliding mode reaching rate effectively optimizes the chattering. Finally, Section 6 provides a summary section.

## 2. Mathematical Model

Generally, the voltage equations of PMSM in the stationary two-phase coordinate system are:

$$\begin{bmatrix} u_\alpha \\ u_\beta \end{bmatrix} = \begin{bmatrix} R + pL_d & \omega_e(L_d - L_q) \\ -\omega_e(L_d - L_q) & R + pL_q \end{bmatrix} \begin{bmatrix} i_\alpha \\ i_\beta \end{bmatrix} + \begin{bmatrix} E_\alpha \\ E_\beta \end{bmatrix} \quad (1)$$

where  $L_d$  and  $L_q$  are stator inductances,  $R$  is the stator resistance,  $\omega_e$  is the electrical angular velocity,  $p$  is the differential operator,  $u_\alpha$  and  $u_\beta$  are the stator voltages,  $i_\alpha$  and  $i_\beta$  are the stator currents, and  $E_\alpha$  and  $E_\beta$  are the back electromotive forces, which satisfy:

$$\begin{bmatrix} E_\alpha \\ E_\beta \end{bmatrix} = [(L_d - L_q)(\omega_e i_d - p i_q) + \omega_e \varphi_f] \begin{bmatrix} -\sin\theta_e \\ \cos\theta_e \end{bmatrix} \quad (2)$$

where  $\varphi_f$  is the magnetic flux,  $\theta_e$  is the electrical angle of the motor,  $\omega_e$  is the electrical angular velocity of the motor, and  $i_d$  and  $i_q$  are the DC current components of the motor on the d-q axis. The dq coordinate system is derived from a rotational, in which the d-axis aligns with the direction of the magnetic field, while the q-axis is perpendicular to it. For a surface-mounted PMSM (SPMSM) with  $L_q = L_d = L_s$ , Equation (2) of the back

electromotive force can be simplified to variables only related to the motor speed and the position angle, as shown in Equation (3):

$$\begin{bmatrix} E_\alpha \\ E_\beta \end{bmatrix} = \omega_e \varphi_f \begin{bmatrix} -\sin\theta_e \\ \cos\theta_e \end{bmatrix} \quad (3)$$

For an interior PMSM (IPMSM) with  $L_q \neq L_d$ , it can be seen from the above Equation (2) that the back electromotive force is not only related to the motor speed, but also to the stator current  $i_d$  and the differential of the stator current  $pi_q$ . This means that the load state of the motor will affect the back electromotive force. Under high-speed and overload conditions of motor operation, the stator current undergoes significant changes, becoming an important component of the back electromotive force distortion.

The motion equations for PMSM are as follows:

$$J \frac{d\omega_m}{dt} = T_e - T_L - B\omega_m \quad (4)$$

$$T_e = \frac{3}{2} p_n i_q [i_d (L_d - L_q) + \varphi_f] \quad (5)$$

where  $\omega_m$  is the motor mechanical angular velocity,  $J$  is the moment of inertia,  $p_n$  is the number of pole pairs,  $B$  is the damping coefficient, and  $T_e$  and  $T_L$  are the electromagnetic torque and load torque, respectively.

The remaining content in this article adopts the model of surface-mounted PMSM (SPMSM) with  $L_q = L_d = L_s$ , and combines it with Matlab/Simulink for analysis.

### 3. Design of Improved Reaching Rate

#### 3.1. Traditional Reaching Rate

For the sliding mode control algorithm, Academician Gao Weibing of China proposed the concept of reaching rate to improve the quality of sliding mode control [26]. There are several main forms of reaching rate, including the constant rate, the exponential rate, and the power rate. Taking the traditional exponential convergence rate as an example:

$$\dot{s} = -\varepsilon \text{sign}(s) - qs, \varepsilon, q > 0 \quad (6)$$

In the equation,  $s$  is the switching function of the sliding mode surface,  $-\varepsilon \text{sign}(s)$  is the constant convergence term, and  $-qs$  is the pure exponential convergence term. When the system state point lies on the sliding mode surface, its motion trajectory is primarily governed by the pure exponential term. As the state point approaches the sliding mode surface, the magnitude of the pure exponential term gradually diminishes until it ultimately converges to zero. After that, the motion trajectory is mainly determined by the constant term.  $\varepsilon$  and  $q$  are the coefficients of the two convergence terms. Increasing  $\varepsilon$  and  $q$  speeds increases the convergence motion, while decreasing them slows down the convergence rate. However, large  $\varepsilon$  and  $q$  will inevitably increase the system's chattering level. Reasonable adjustment and selection of these two coefficients are particularly important to ensure that the system effectively reduces chattering and increases the convergence rate.

When  $s > 0$  in the expression of the constant convergence term,  $\text{sign}(s) = 1$  is true. And because both  $\varepsilon$  and  $q$  are greater than 0, the derivative of the function with respect to  $s$  becomes negative. The function of  $s$  is decreasing, causing the system's state point to move towards the sliding surface along its motion trajectory. When  $s < 0$ , there is  $\text{sign}(s) = -1$ , and  $s$  is an increasing function. Similarly, under the effect of the reaching rate, the motion trajectory moves towards the sliding surface. According to Equation (6), the convergence time required for the system state trajectory to reach the sliding surface can be obtained.

$$t = \frac{|s_0|}{\varepsilon} \quad (7)$$

From Equation (7), it can be seen that the calculation of the convergence time is directly related to the value of  $\epsilon$ . If the value of  $\epsilon$  increases, the convergence time will decrease and the robustness will improve. However, this will cause the system's chattering to increase, resulting in a conflict between the system chattering and the convergence time of the sliding surface due to the value of  $\epsilon$ .

### 3.2. Improved Reaching Rate

A new reaching rate has been designed considered the shortcomings of the traditional reaching rates in combination with the latest research from references [22,24].

$$\dot{s} = -k_s \text{sign}(s) - k_1 s \tag{8}$$

$$k_s = \frac{k \cdot E^2}{\epsilon + (1 - \epsilon)e^{-\alpha|s|}} \tag{9}$$

The design of this reaching rate selects the exponential term  $k_1 s$ , the exponential term  $e^{-\alpha|s|}$ , and the  $E^2$  term, which can increase the convergence rate while also determining the coefficient size in real-time based on the system state, demonstrating a certain degree of time-varying behavior.  $k_1 s$  is the purely exponential reaching term; when the state point of the system is away from the sliding surface, the reaching motion is mainly determined by it. When  $|s|$  is large,  $k_s$  is approximately equal to  $\frac{k \cdot E^2}{\epsilon}$  and can better approach the sliding surface with changes in error.  $k_s$  is much larger than the initial base  $k$ , and the controlled system is quickly forced to converge to the sliding mode surface with the help of the linear gain  $k_1$ . As the system's state point gradually approaches the sliding mode surface,  $k_s$  is approximately equal to  $k \cdot E^2$ , finally, and the initial base value  $k$  under the effect of  $E^2$  and  $k_1$  ensures that the motion trajectory of the system has less chattering, guaranteeing the quality of the system.

**Theorem 1.** For the improved convergence rate  $\dot{s} = -k_s \text{sign}(s) - k_1 s$  with  $k_s = \frac{k \cdot E^2}{\epsilon + (1 - \epsilon)e^{-\alpha|s|}}$ , it can converge stably to the sliding mode surface only when  $k > 0$ .

**Proof of Theorem 1.** According to the Lyapunov stability principle, a Lyapunov function is selected:

$$V = \frac{1}{2} s^2 \tag{10}$$

The sliding mode reaching condition is satisfied only when  $\dot{V} < 0$ .

$$\dot{V} = s\dot{s} = -s \cdot \frac{k \cdot E^2}{\epsilon + (1 - \epsilon)e^{-\alpha|s|}} \cdot \text{sign}(s) - k_1 s^2 \tag{11}$$

From Equation (11), it can be seen that, since  $s \cdot \text{sign}(s) \geq 0$ ,  $\dot{V} < 0$  holds when  $k > 0$ , which ensures that the system's state point gradually moves to the sliding surface and reaches the origin in a finite time.

A quantitative analysis is conducted to determine the reaching rate for the aforementioned process, with the aim of calculating the convergence time required to reach the sliding surface.

From Equations (8) and (9), we obtain:

$$\dot{s} = - \frac{k \cdot E^2}{\epsilon + (1 - \epsilon)e^{-\alpha|s|}} \text{sign}(s) - k_1 s \tag{12}$$

Let  $S_0$  be much larger than 1 at  $t = 0$ , and let  $D = - \frac{k \cdot E^2}{\epsilon + (1 - \epsilon)e^{-\alpha|s|}} \text{sign}(s)$ ; then, we have:

$$D \approx \frac{-kE^2}{\epsilon} \tag{13}$$

then:

$$\dot{s} + k_1 s = D \tag{14}$$

solving it gives, where C is an arbitrary constant:

$$s = e^{-k_1 t} \left( \frac{D}{k_1} e^{k_1 t} + C \right) \tag{15}$$

substituting  $S_0$  into it, we obtain:

$$C = S_0 - \frac{D}{k_1} \tag{16}$$

at this point, if we let  $s = 0$ , then, we have:

$$t_1 = \frac{\ln \left| -\frac{D}{(S_0 - \frac{D}{k_1})k_1} \right|}{k_1} \tag{17}$$

□

From Equation (17), it can be concluded that the system's state point converges to the sliding surface after  $t_1$  time.

#### 4. Construction of System

The modeling in this paper is based on a surface-mounted, three-phase permanent magnet synchronous motor ( $L_d = L_q$ ). Equation (1) can be transformed into the current equation as follows:

$$p \begin{bmatrix} i_\alpha \\ i_\beta \end{bmatrix} = -\frac{R}{L_s} \begin{bmatrix} i_\alpha \\ i_\beta \end{bmatrix} + \frac{1}{L_s} \begin{bmatrix} u_\alpha \\ u_\beta \end{bmatrix} - \frac{1}{L_s} \begin{bmatrix} E_\alpha \\ E_\beta \end{bmatrix} \tag{18}$$

To obtain an estimation of the back electromotive force, the SMO design is typically as follows:

$$p \begin{bmatrix} \hat{i}_\alpha \\ \hat{i}_\beta \end{bmatrix} = -\frac{R}{L_s} \begin{bmatrix} \hat{i}_\alpha \\ \hat{i}_\beta \end{bmatrix} + \frac{1}{L_s} \begin{bmatrix} u_\alpha \\ u_\beta \end{bmatrix} - \frac{1}{L_s} \begin{bmatrix} \hat{E}_\alpha \\ \hat{E}_\beta \end{bmatrix} \tag{19}$$

where  $\hat{i}_\alpha$  and  $\hat{i}_\beta$  are the observed stator currents, and  $u_\alpha$  and  $u_\beta$  are the control inputs of the observer. The stator current error equation is obtained by subtracting the above two equations:

$$p \begin{bmatrix} \tilde{i}_\alpha \\ \tilde{i}_\beta \end{bmatrix} = -\frac{R}{L_s} \begin{bmatrix} \tilde{i}_\alpha \\ \tilde{i}_\beta \end{bmatrix} + \frac{1}{L_d} \begin{bmatrix} \hat{E}_\alpha - E_\alpha \\ \hat{E}_\beta - E_\beta \end{bmatrix} \tag{20}$$

The equations  $\hat{i}_\alpha - i_\alpha = \tilde{i}_\alpha$  and  $\hat{i}_\beta - i_\beta = \tilde{i}_\beta$  are used, and the sliding mode reaching rate Equations (8) and (9) are introduced into the design.

$$\begin{bmatrix} \hat{E}_\alpha \\ \hat{E}_\beta \end{bmatrix} = \begin{bmatrix} -k_s \text{sign}(s_\alpha) - k_1 s_\alpha \\ -k_s \text{sign}(s_\beta) - k_1 s_\beta \end{bmatrix} \tag{21}$$

where  $s_\alpha = \hat{i}_\alpha - i_\alpha$ ,  $s_\beta = \hat{i}_\beta - i_\beta$ .

When the state variables of the observer reach the sliding surface, we have  $\tilde{i}_\alpha = \tilde{i}_\beta = 0$ . According to the equivalent control principle of sliding mode control, the control input at this time can be regarded as an equivalent control input, that is:

$$\begin{bmatrix} E_\alpha \\ E_\beta \end{bmatrix} = \begin{bmatrix} \hat{E}_\alpha \\ \hat{E}_\beta \end{bmatrix} = \begin{bmatrix} -k_s \text{sign}(s_\alpha) - k_1 s_\alpha \\ -k_s \text{sign}(s_\beta) - k_1 s_\beta \end{bmatrix} \tag{22}$$

Then, after estimating the back electromotive force of the motor, the rotor position and speed information can be obtained through the arctangent function, that is:

$$\theta_e = -\arctan\left(\frac{\hat{E}_\alpha}{\hat{E}_\beta}\right) \tag{23}$$

$$\hat{\omega}_e = \frac{d\theta_e}{dt} \tag{24}$$

where  $\theta_e$  is the electrical angle, and  $\hat{\omega}_e$  is the estimated electrical angular velocity. In summary, the structure of the SMO based on the improved SM reaching rate is shown in Figure 1. Because the control signal is a discontinuous high-frequency switching signal, it is necessary to input the estimated value of the back electromotive force obtained by the SMO into a low-pass filter for filtering. Similarly, since  $\hat{\omega}_e$  is also obtained through differentiation, a low-pass filter is applied to remove the high-frequency noise caused by differentiation.

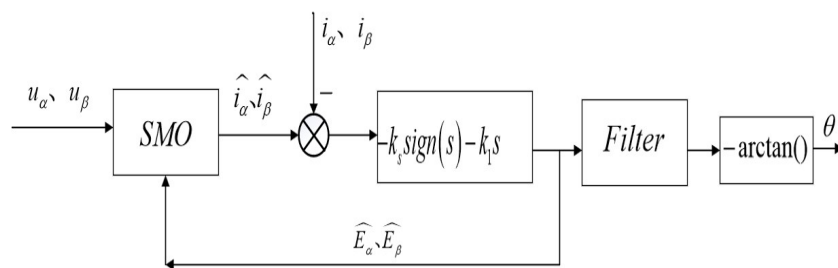


Figure 1. Structure of SMO.

Then, the rotor angle position can be determined using the inverse tangent function. Subsequently, the acquired position information is integrated with the inverse Park transformation to finalize the establishment of the control system. Figure 2 illustrates the configuration of the PMSM control system featuring the improved SMO and SMC algorithm. The system primarily comprises a speed loop and a current loop, employing SMC for speed regulation. In order to establish the sliding mode speed controller, system state variables are selected:

$$\begin{cases} x_1 = \omega_m^* - \omega_m \\ x_2 = \dot{x}_1 = -\dot{\omega}_m \end{cases} \tag{25}$$

The mathematical model of PMSM in the d-q axis coordinate system based on the equations is:

$$\begin{cases} \dot{x}_1 = -\dot{\omega}_m = \frac{1}{J}(T_L - \frac{3p_n\phi_f}{2}i_q) \\ \dot{x}_2 = -\ddot{\omega}_m = -\frac{3p_n\phi_f}{2J}\dot{i}_q \end{cases} \tag{26}$$

let  $D = \frac{3p_n\phi_f}{2J}, u = \dot{i}_q$ ; the state space equation for it is:

$$\begin{bmatrix} \dot{x}_1 \\ \dot{x}_2 \end{bmatrix} = \begin{bmatrix} 0 & 1 \\ 0 & 0 \end{bmatrix} \begin{bmatrix} x_1 \\ x_2 \end{bmatrix} + \begin{bmatrix} 0 \\ -D \end{bmatrix} u \tag{27}$$

The sliding surface is defined as  $s = cx_1 + x_2$ , where  $c > 0$ . Solving it:

$$\dot{s} = cx_1 + \dot{x}_2 = cx_2 - Du \tag{28}$$

combining Equations (8) and (9) and integrating, we get:

$$i_q = \frac{1}{D} \int [cx_2 + k_s \text{sign}(s) + k_1 s] dt \tag{29}$$

The input of the speed error can be transformed into  $i_q^*$  through the utilization of SMC; thus, the construction of the SM controller is completed.

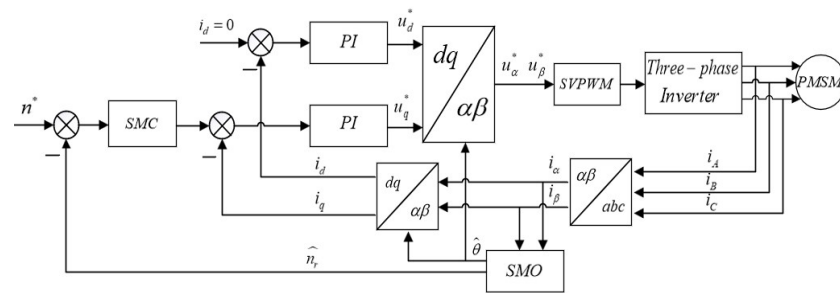


**Figure 2.** Structure of the sensorless control system for PMSM based on improved SM reaching rate.

## 5. Simulation and Experimental

### 5.1. Simulation and Comparison

#### 5.1.1. Simulation Modeling

The parameters of the PMSM used in the simulation are consistent with those used on the towing test bench, as shown in Table 1. For the parameter selection of the sliding mode algorithm, the values of  $k$  and  $k_1$  determine the convergence rate. To ensure that the system has a shorter convergence time, larger values are first selected. The values of  $\alpha$  and  $\varepsilon$  affect the value of  $k_s$ , which, in turn, determines the dynamic response performance of the system. The four parameters  $k$ ,  $k_1$ ,  $\alpha$ , and  $\varepsilon$  are mutually coordinated, and each parameter is adjusted sequentially to stabilize the waveform of the system output. The simulation's duration is limited to 2 s to ensure comprehensive observation of the motor's state curves during operation. Considering the suitability of the observer-based sensorless control method for medium- and high-speed ranges, the reference speed is set at 1000 rpm. To assess and validate the robustness of the control system, sudden loads of 1 N·m and 3 N·m are introduced at 0.1 s and 0.6 s, respectively, considering that the motor's rated torque is 2.4 N·m. The performance of the system is evaluated based on the simulation results.

**Table 1.** Parameters of PMSM

Parameters	Values
Number of poles $p_n$	5
Stator inductance $L_s$ /mH	6.552
Stator resistance $R/\Omega$	0.901
Flux $\varphi_f$ /Wb	0.06912
Damping factor	$8.4 \times 10^{-5}$
Inertia $J/(\text{kg}\cdot\text{m}^2)$	$1.2 \times 10^{-4}$
Rated torque (N·m)	2.4
Peak torque (N·m)	7.2

The speed curve, which is based on the improved sliding mode algorithm portrayed in Figure 3a, depicts a simulation of the output speed behavior of the system. The results illustrate that the system exhibits rapid acceleration towards the reference speed. However, when a load of 1 N·m is introduced, there is a notable decrease in the output speed. Nevertheless, after a short adjustment period, the system effectively returns to the set speed even under load conditions. Similarly, when subjected to a load of 3 N·m, the system demonstrates its capability to recover and maintain the desired set speed. An examination of the output torque curve presented in Figure 3b provides further evidence that the system employing the improved sliding mode reaching rate operates efficiently, enabling sensorless control of PMSM.

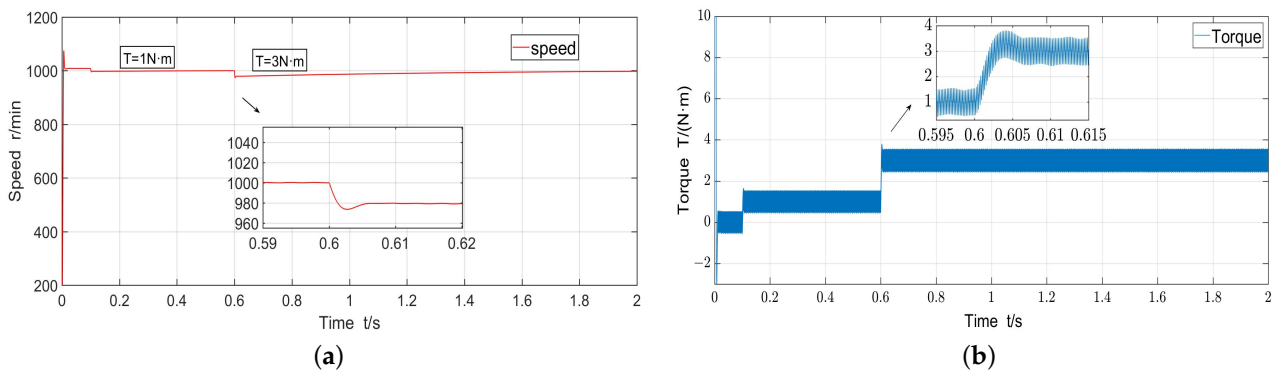


**Figure 3.** Curves of the output from system: (a) Speed curve based on the improved SM reaching rate, (b) Torque curve based on the improved SM reaching rate.

### 5.1.2. Comparisons of SM Algorithms

This subsection compares the performance of the traditional SM algorithm, the replicated SM algorithm from reference [24], and the improved SM algorithm. The three SM algorithms are simulated under identical external conditions. The reference speed is uniformly set to 1000 rpm in all cases. Moreover, a sudden additional load of 1 N·m is applied at 0.1 s, followed by a subsequent increase to 3 N·m at 0.6 s. Figure 4 illustrates the comparative graph of the output speeds for the three algorithms.

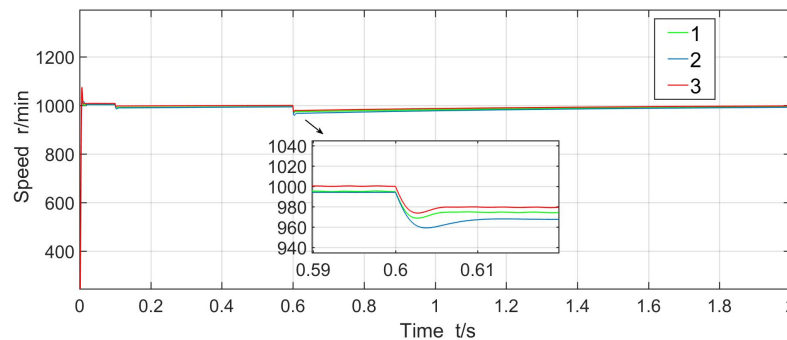


**Figure 4.** Comparison of the output speed curves for the three algorithms.

Figure 4 illustrates the speed curves of the control system, with curves 1, 2, and 3 representing the traditional algorithm, the one replicated from the literature, and the improved algorithm proposed in this paper, respectively. The figure clearly demonstrates that all three algorithms rapidly achieve the set speed for the system. Curve 3, corresponding to the improved algorithm proposed in this paper, exhibits a slightly higher steady-state error compared to curves 1 and 2. However, when a sudden load is introduced, the improved SM algorithm demonstrates superior anti-interference capability compared to curves 1 and 2. Firstly, curve 3 experiences a smaller speed drop compared to the other two, and it also requires less time to recover to the set speed after the drop. In the context of a sudden increase in load, the system demonstrates good robustness performance.

According to the structure of the sensorless control system for PMSM depicted in Figure 2, the control system employs a sliding mode observer to observe and estimate the output speed, thereby facilitating the development of a closed-loop speed control system. By utilizing the angle information provided by the observer, the system establishes a closed-loop current control. To evaluate the performance of the sliding mode observer constructed using an improved sliding mode algorithm, the errors between the actual angle and the estimated angle by the observer, as well as the errors between the system’s output speed and the estimated speed by the observer, are selected for comparative analysis. The comparative results are presented in Figure 5.

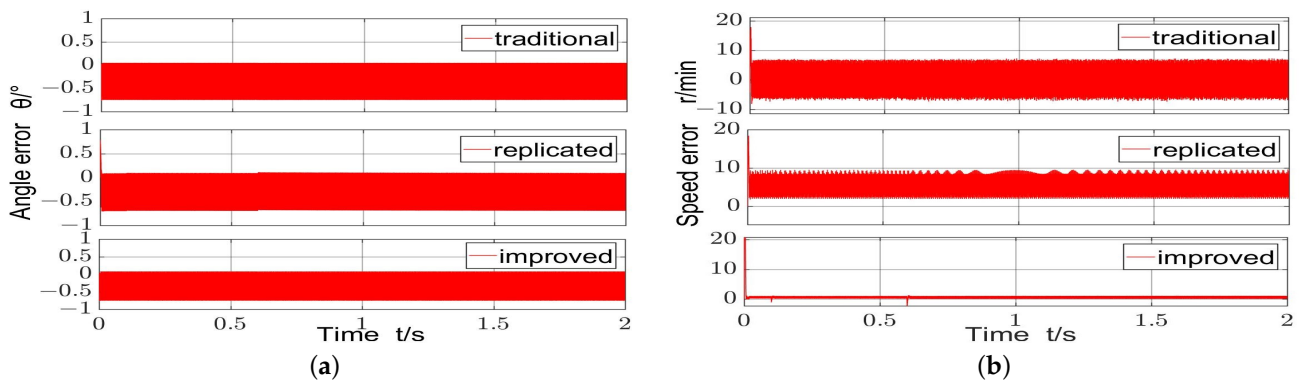


**Figure 5.** Curves of the three observers regarding: (a) the error of the angle, (b) the error of the speed.

In Figure 5a, a comparison is presented among three observers based on the angle information they directly output. The graph clearly shows no significant difference among the three observers, as all of them are capable of accurately estimating the angle information of the rotor. However, in Figure 5b, it is evident that the improved sliding mode algorithm demonstrates a clear advantage in speed tracking error. It has the smallest speed tracking error, even in the presence of disturbances like a sudden additional load.

In order to facilitate a comprehensive comparison between the observer and the speed controller, three specific values have been chosen: the reference current  $i_q^*$  generated by the speed controller, and the estimated  $i_q$  and the  $i_d$  values derived from the angle information provided by the observer. The three values resulting from the three different convergence rates are then compared (note that the  $i_d^*$  comparison is not selected due to the adoption of the  $i_d^* = 0$  strategy), as depicted in Figure 6.

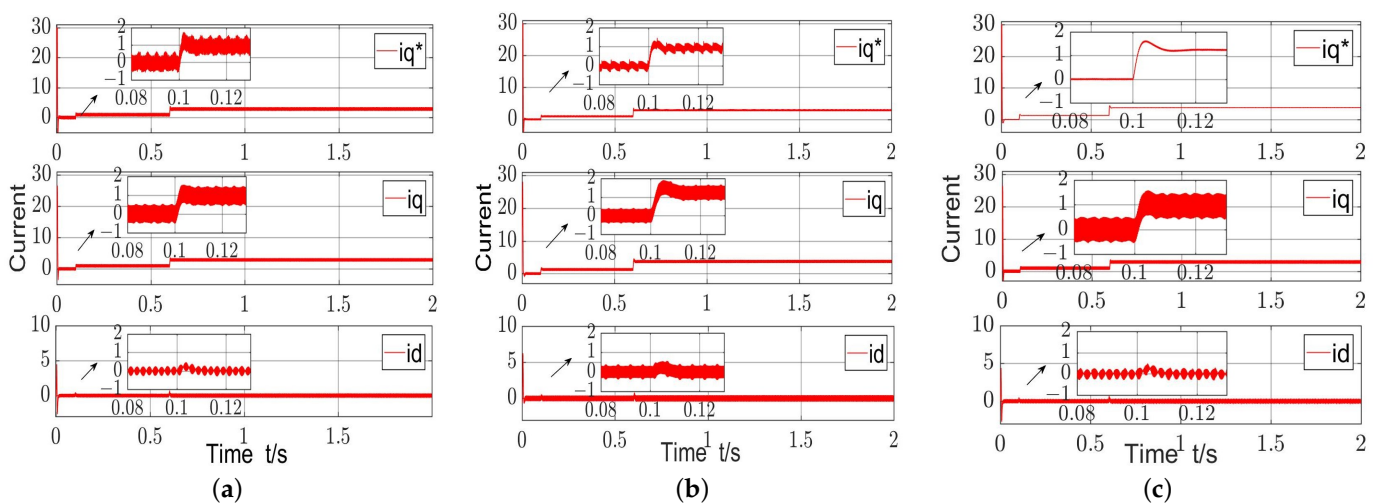


**Figure 6.** Curves of current  $i_q^*$ ,  $i_q$ ,  $i_d$ : (a) traditional SM reaching rate, (b) replicated SM reaching rate, (c) improved SM reaching rate.

In this context,  $i_d$  represents the excitation-current-producing component in the motor, while  $i_q$  represents the torque-producing component. Figure 6 demonstrates that the replicated sliding mode reaching rate exhibits reduced chattering in  $i_q^*$  when compared to the traditional algorithm, which has some significance in terms of optimization. However, the improved sliding mode reaching rate proposed in this paper yields a more substantial enhancement in chattering optimization for  $i_q^*$ . When comparing  $i_d$ , although the replicated sliding mode reaching rate can partially reduce chattering on  $i_q^*$ , its estimation performance for  $i_d$  is inferior to that of the conventional sliding mode reaching rate. Uti-

lizing an improved sliding mode reaching rate not only significantly impacts  $i_q^*$ , but also demonstrates equal effectiveness in estimating  $i_d$ .

## 5.2. Experimental Verification

### 5.2.1. Construction of Towing Test Platform

A towing test bench was established for PMSM, comprising two motors rated at 750 W each, interconnected through a coupling. One motor was utilized for driving, while the other operated in the opposite direction to serve as a load. The field-oriented control (FOC) algorithm is employed to regulate the driving current of the load motor, enabling torque control. The algorithm was validated through experiments conducted on the towing bench. The control board utilized the DSP28335 chip to control the motors, while the upper computer controlled and implemented the loading motor for applying the load. Once the program was compiled in the CCS5.5 software, it was downloaded to the chip using a simulator and subsequently powered up to verify its functionality. The experimental data were collected using the DSP28335 chip and communicated with the upper computer. Figure 7 illustrates the structural diagram of the towing test bench.

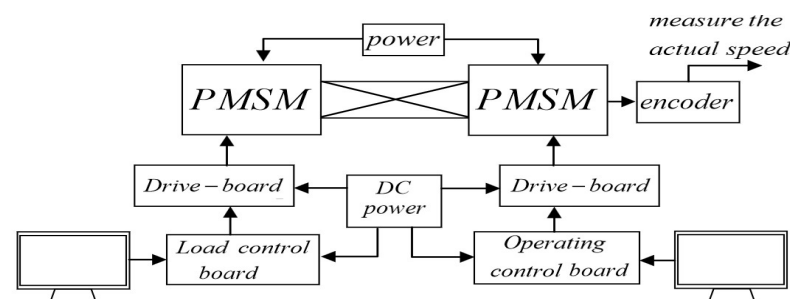


Figure 7. Structure of the Towing Test bench.

The experimental setup, as illustrated in Figure 8, involves the utilization of software to program and upload control algorithms to the control board. Both the control board and driver board operate on a 24 V DC power supply to facilitate motor control. The primary function of the control board is to regulate the driver board, enabling the implementation of SVPWM. To measure the speed of the system, an encoder is employed, providing data for comparison. Additionally, the control board has the capability to transmit the collected data to the software for further analysis and evaluation.

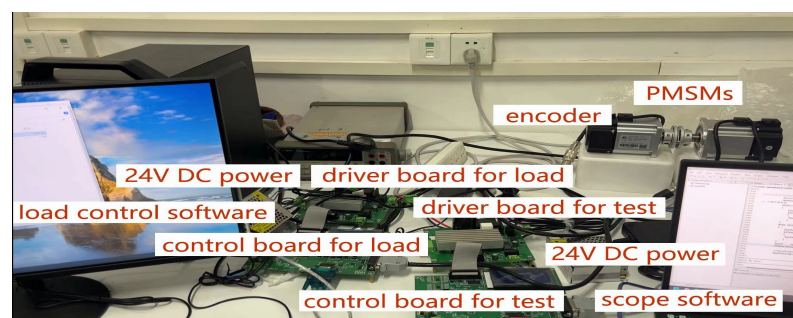
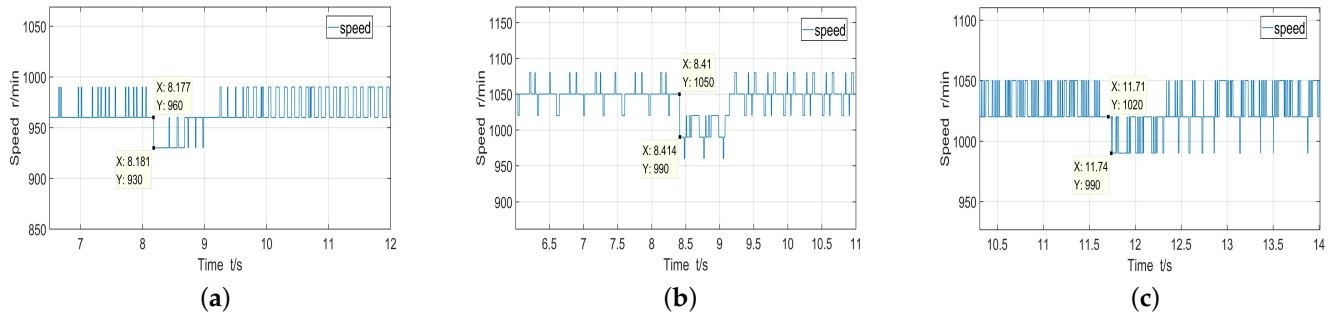


Figure 8. Devices of the Towing Test bench.

### 5.2.2. Comparative Experiment

A towing test bench was utilized to conduct experimental investigations aimed at evaluating the performance of the sensorless control systems for PMSM employing three distinct sliding mode algorithms. Consistent with the simulations, the external conditions were maintained unchanged throughout the experiments. Initially, a sudden additional load of 1 N·m was applied to the motor while it was in operation. Subsequently, the motor was subjected to running conditions under load. The objective of the experimental study

was to observe and analyze the motor's running state in order to assess the performance related to various sliding mode reaching rates. The speed of system output was selected for comparative analysis, as shown in Figure 9.



**Figure 9.** Speed curves of the three algorithms under the 1 N·m load: (a) traditional SM reaching rate, (b) replicated SM reaching rate, (c) improved SM reaching rate.

Figure 9a–c show the output speed of the motor under different SM algorithms with a sudden load of 1 N·m. As shown in Figure 9a, the output speed of the motor ranges from 960 to 990 rpm when employing the traditional sliding mode reaching rate. It exhibits a slight deviation of  $-1\sim-4\%$  compared to the reference speed of 1000 rpm. After a sudden load disturbance, the output speed decreases by 30 rpm but recovers within approximately 1.1 s under loaded conditions. Figure 9b illustrates that employing the replicated sliding mode reaching rate results in an output speed ranging from 1020 to 1080 rpm, with an error range of  $+2\sim+8\%$  compared to the reference speed. After a sudden load disturbance, the output speed decreases by 60 rpm but recovers within approximately 0.8 s under loaded conditions. The effect of the improved sliding mode reaching rate is depicted in Figure 9c, resulting in an output speed ranging from 1020 to 1050 rpm with an error range of  $+2\sim+5\%$  compared to the reference speed. After a sudden load disturbance, the output speed decreases by 30 rpm but recovers within approximately 0.6 s under loaded conditions.

In the sensorless control system of PMSM, the q-axis current is of significant importance as it reflects the control performance of the system. Figure 10 illustrates that the control system utilizing the replicated SM reaching rate results in a higher level of chattering in the q-axis current following sudden load changes. This finding aligns with the simulation results, indicating that the replicated SM algorithm leads to an increased q-axis current. While this can enhance the torque output capability of the motor, it concurrently introduces elevated power losses, heat generation, and has potential impacts on the stability of the overall system. In contrast, the improved SM reaching rate demonstrates reduced chattering in the q-axis current, suggesting enhanced stability.

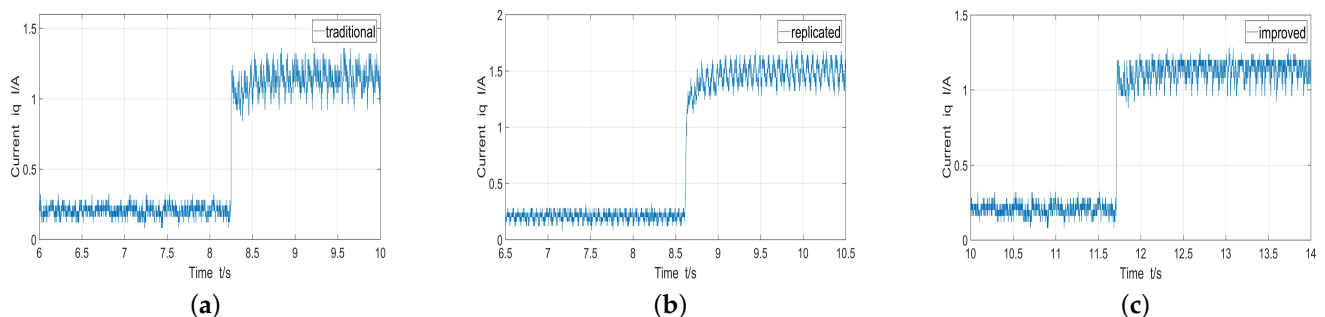


**Figure 10.** Current  $i_q$  curves of the three algorithms under the 1 N·m load: (a) traditional SM reaching rate, (b) replicated SM reaching rate, (c) improved SM reaching rate.

Next, the control system is experimentally evaluated using three different algorithms in order to validate the effectiveness of the improved sliding mode reaching rate and assess the performance of the SMO and SMC. Specifically, a change is made from 1 N·m to 3 N·m, and the resulting estimated output speed obtained through the algorithms is compared with the real-time speed obtained from an encoder. The experimental results are presented in Figure 11.

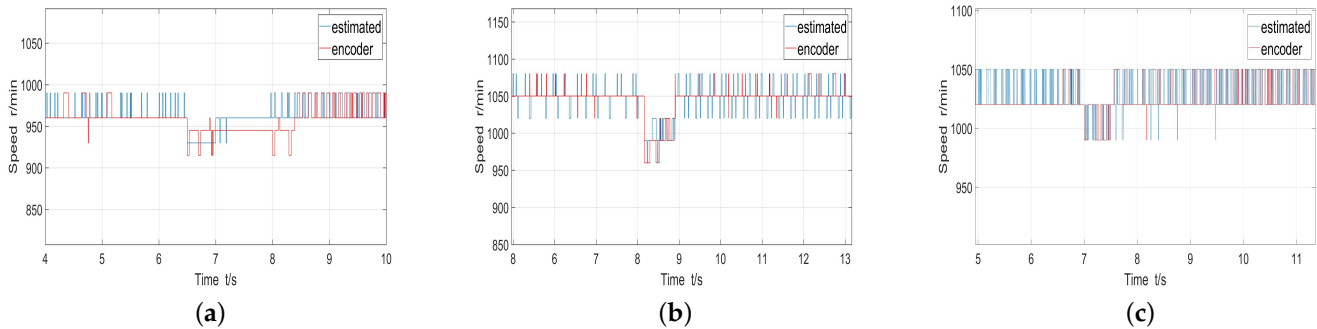


**Figure 11.** Comparison curves between estimated speed and real-time speed of the three algorithms under 3 N·m: (a) traditional SM reaching rate, (b) replicated SM reaching rate, (c) improved SM reaching rate.

In Figure 11a, the output speed experiences a decrease of 30 rpm when subjected to a sudden 3 N·m load under the influence of the traditional SM reaching rate. The recovery time under loaded conditions is approximately 1.5 s. In Figure 11b, the implementation of the replicated SM reaching rate results in a larger decrease of 60 rpm in the output speed after the sudden load. However, the speed recovers more quickly, taking approximately 0.8 s under loaded conditions. Similarly, in Figure 11c, the improved SM reaching rate leads to a decrease of 30 rpm in the output speed after the sudden load, with a faster recovery time of approximately 0.6 s under loaded conditions. Examining the comparison between the estimated speed and real-time speed, Figure 11a reveals errors between the estimated output speed and the actual speed in the control system employing the traditional SM reaching rate. The tracking performance of the speed estimated by the SMO is poor, as it fails to closely match the real-time speed curve. However, Figure 11b,c demonstrate that the control systems utilizing the replicated SM reaching rate and the improved SM reaching rate, respectively, exhibit superior tracking performance.

In order to comprehensively assess the effectiveness of the control system, we have chosen to evaluate the output torque of the motor at a load of 3 N·m for comparative purposes. Figure 12 visually presents the various control systems implemented using three distinct sliding mode algorithms.

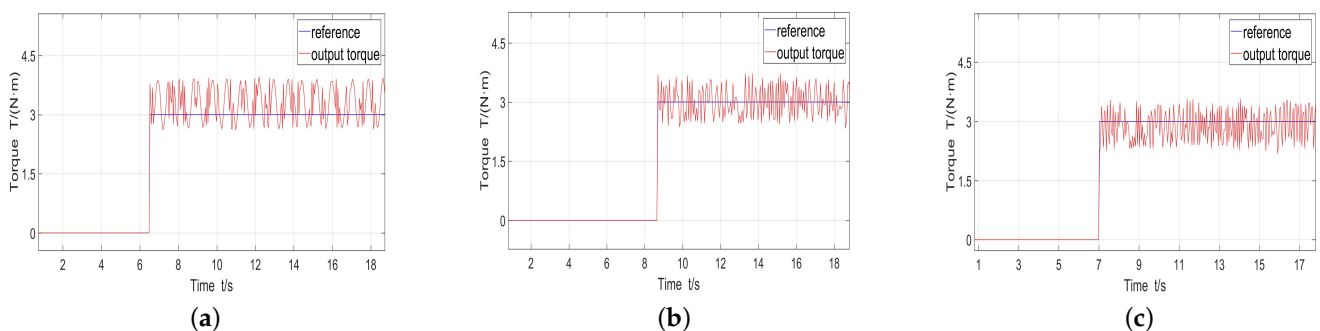


**Figure 12.** Comparison curves between reference load torque and output torque of the three algorithms under 3 N·m: (a) traditional SM reaching rate, (b) replicated SM reaching rate, (c) improved SM reaching rate.

Figure 12 clearly illustrates the prompt response of all three control systems to abrupt load variations. However, it is noteworthy that the control system employing the traditional reaching rate exhibits a significantly higher maximum amplitude in the output torque curve. This observation suggests potential deficiencies in its disturbance rejection capability. In contrast, both the replicated sliding mode algorithm and the improved sliding mode algorithm show robustness in their performance.

Figure 13 presents a comparison of the real rotor position and the estimated rotor position by the improved SMO. The real rotor position is measured by an encoder. From the experimental results, the estimating error is less than 0.1 rad, meaning that the improved SMO can estimate the rotor position precisely. The result is calculated from the SMO, which is filtered by LPF, so that a precise value can be obtained. Combined with the experimental results for the rotor position comparison and the speed error comparison, the performance of the improved SMO can be illustrated.

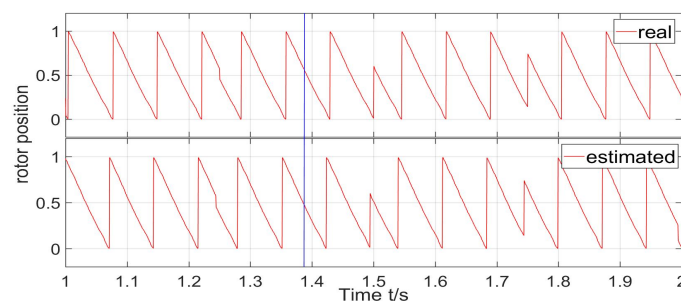


**Figure 13.** Real and estimated rotor position of the improved SM algorithm under 1000 rpm.

In order to make the results more clear, the diverse data are presented in Table 2, as depicted below.

**Table 2.** Experimental Data Comparison Table.

	Traditional	Replicated	Improved
Speed range	960–990 r/min	1020–1080 r/min	1020–1050 r/min
Speed drop under 1 N·m	30 r/min	60 r/min	30 r/min
Recovery time under 1 N·m	1.1 s	0.8 s	0.6 s
q-axis current under 1 N·m	$1.16 \pm 0.2$ A	$1.5 \pm 0.18$ A	$1.12 \pm 0.16$ A
Speed drop under 3 N·m	30 r/min	60 r/min	30 r/min
Recovery time under 3 N·m	1.5 s	0.8 s	0.6 s

The improved sliding mode reaching rate algorithm demonstrates superior performance compared to the traditional and replicated sliding mode algorithms in terms of speed chattering. Specifically, it exhibits the smallest speed chattering range of 30 r/min. When subjected to a sudden load of 1 N·m, the speed decrease observed in the control system employing the improved sliding mode reaching rate algorithm is equivalent to that of the traditional algorithm, both resulting in a speed decrease of 30 r/min. This is in contrast to the replicated sliding mode algorithm, which leads to a larger speed decrease of 60 r/min. Furthermore, the improved algorithm achieves a shorter recovery time under the sudden load of 1 N·m. Similarly, when subjected to a sudden load of 3 N·m, the improved algorithm outperforms both the traditional and replicated algorithms by exhibiting a shorter recovery time. Analysis of the q-axis current data under the 1 N·m load reveals that the improved sliding mode algorithm effectively reduces chattering, indicating enhanced stability. Moreover, Figure 11 demonstrates that the control system utilizing the improved sliding mode algorithm offers superior tracking performance.

## 6. Conclusions

This paper aims to address the issue of output chattering in sliding mode algorithms by proposing an optimization technique for the sliding mode reaching rate. The proposed approach introduces an error term to improve the algorithm's performance. Specifically, the study focuses on developing a sensorless control system for a PMSM using a combination of SMC and SMO. The primary objective of this control system is to minimize output chattering.

To validate the effectiveness of the proposed system, both simulations and experiments are conducted. The obtained experimental results demonstrate that the system successfully reduces the range of output speed chattering to within +2~+5%. This outcome indicates the feasibility of the proposed system and its significant impact on reducing chattering.

However, it is important to acknowledge that the current implementation of the system is limited to medium- and high-speed ranges. Thus, future research will focus on extending the control capabilities of the system to cover the full speed range. By addressing this limitation, a more comprehensive and versatile control solution can be achieved.

**Author Contributions:** Methodology, Y.C. and A.L.; software, X.Y. and A.L.; validation, Y.C., X.Y. and A.L.; data curation, A.L.; writing—original draft preparation, A.L.; writing—review and editing, Y.C., A.L., H.L., X.Y. and W.C. All authors have read and agreed to the published version of the manuscript.

**Funding:** Supported by the National Key R&D Program of China (2021YFB3901300).

**Data Availability Statement:** Not applicable.

**Conflicts of Interest:** The authors declare no conflict of interest.

## References

1. Vaez-Zadeh, S. *Control of Permanent Magnet Synchronous Motors*; Oxford University Press: Oxford, UK, 2018. [\[CrossRef\]](#)
2. Liu, J.L.; Xiao, F.; Shen, Y.; Mai, Z.Q.; Li, C.R. Research review on Sensorless control technology of permanent magnet synchronous motor. *J. Electrotech. Eng.* **2017**, *32*, 76–88. [\[CrossRef\]](#)
3. Zhang, G.Q.; Wang, G.L.; Xu, D.G. Saliency-based position sensorless control methods for PMSM drives—A review. *Chin. J. Electr. Eng.* **2017**, *3*, 14–23. [\[CrossRef\]](#)
4. Liu, Z.H.; Nie, J.; Wei, H.L.; Chen, L.; Wu, F.M. Second-order ESO-based current sensor fault-tolerant strategy for sensorless control of PMSM with B-phase current. *IEEE/ASME Trans. Mechatron.* **2022**, *27*, 5427–5438. [\[CrossRef\]](#)
5. Yin, Z.G.; Li, W.; Zhang, Y.Q.; Tang, R.J. Model predictive torque control based on a disturbance observer for induction motor drives. In Proceedings of the 2019 14th IEEE Conference on Industrial Electronics and Applications (ICIEA), Xi'an, China, 19–21 June 2019; pp. 1871–1875. [\[CrossRef\]](#)
6. Apte, A.; Joshi, V.A.; Mehta, H.; Walambe, R. Disturbance-observer-based sensorless control of PMSM using integral state feedback controller. *IEEE Trans. Power Electron.* **2019**, *35*, 6082–6090. [\[CrossRef\]](#)
7. Lu, X.Q.; Lin, H.Y.; Han, J.L. The disturbance observer of permanent magnet synchronous motor controlled without position sensor. *Chin. J. Electr. Eng.* **2016**, *36*, 1387–1394. [\[CrossRef\]](#)
8. Zhou, Y.; Tang, J.; Sheng, M.L.; Zhang, T.; Liu, C. Sensorless control of permanent magnet synchronous motor based on extended state observer. *Micromotor* **2018**, *51*, 44–49. [\[CrossRef\]](#)
9. Chen, S.; Ding, W.; Hu, R.M.; Wu, X.; Shi, S. Sensorless Control of PMSM Drives Using Reduced Order Quasi Resonant-Based ESO and Newton–Raphson Method-Based PLL. *IEEE Trans. Power Electron.* **2022**, *38*, 229–244. [\[CrossRef\]](#)
10. Yu, B.; Shen, A.; Chen, B.; Luo, X.; Tang, Q.; Xu, J.; Zhu, M. A Compensation Strategy of Flux Linkage Observer in SPMSM Sensorless Drives Based on Linear Extended State Observer. *IEEE Trans. Energy Convers.* **2022**, *37*, 824–831. [\[CrossRef\]](#)
11. Zhang, T.; Xu, Z.; Li, J.; Zhang, H.; Gerada, C. A Third-Order Super-Twisting Extended State Observer for Dynamic Performance Enhancement of Sensorless IPMSM Drives. *IEEE Trans. Ind. Electron.* **2020**, *67*, 5948–5958. [\[CrossRef\]](#)
12. Zhang, Y.; Jin, J.; Huang, L. Model-Free Predictive Current Control of PMSM Drives Based on Extended State Observer Using Ultralocal Model. *IEEE Trans. Ind. Electron.* **2021**, *68*, 993–1003. [\[CrossRef\]](#)
13. Volpato, C.J.; Vieira, R.P. Adaptive Full-Order Observer Analysis and Design for Sensorless Interior Permanent Magnet Synchronous Motors Drives. *IEEE Trans. Ind. Electron.* **2021**, *68*, 6527–6536. [\[CrossRef\]](#)
14. Sreejith, R.; Singh, B. Sensorless Predictive Current Control of PMSM EV Drive Using DSOGI-FLL Based Sliding Mode Observer. *IEEE Trans. Ind. Electron.* **2021**, *68*, 5537–5547. [\[CrossRef\]](#)
15. Ye, S.C.; Yao, X.X. An Enhanced SMO-Based Permanent-Magnet Synchronous Machine Sensorless Drive Scheme With Current Measurement Error Compensation. *IEEE J. Emerg. Sel. Top. Power Electron.* **2021**, *9*, 4407–4419. [\[CrossRef\]](#)
16. Xu, W.J.; Qu, S.C.; Zhao, L.; Zhang, H.R. An Improved Adaptive Sliding Mode Observer for Middle- and High-Speed Rotor Tracking. *IEEE Trans. Power Electron.* **2021**, *36*, 1043–1053. [\[CrossRef\]](#)

17. Ren, N.N.; Fan, L.; Zhang, Z. Sensorless PMSM Control with Sliding Mode Observer Based on Sigmoid Function. *J. Electr. Eng. Technol.* **2021**, *16*, 933–939. [[CrossRef](#)]
18. Yin, Z.G.; Zhang, Y.P.; Cao, X.P.; Yuan, D.S.; Liu, J. Estimated Position Error Suppression Using Novel PLL for IPMSM Sensorless Drives Based on Full-Order SMO. *IEEE Trans. Power Electron.* **2022**, *37*, 4463–4474. [[CrossRef](#)]
19. Ding, H.; Zou, X.; Li, J. Sensorless Control Strategy of Permanent Magnet Synchronous Motor Based on Fuzzy Sliding Mode Observer. *IEEE Access* **2022**, *10*, 36743–36752. [[CrossRef](#)]
20. Lu, W.; Zheng, D.; Lu, Y.; Lu, K.; Guo, L.; Yan, W.; Luo, J. New Sensorless Vector Control System With High Load Capacity Based on Improved SMO and Improved FOO. *IEEE Access* **2021**, *9*, 40716–40727. [[CrossRef](#)]
21. Lascu, C.; Andreescu, G.-D. PLL Position and Speed Observer with Integrated Current Observer for Sensorless PMSM Drives. *IEEE Trans. Ind. Electron.* **2020**, *67*, 5990–5999. [[CrossRef](#)]
22. Yang, H.; Tang, J.W.; Chien, Y.R. Application of new sliding mode control in vector control of PMSM. *IEICE Electron. Express* **2022**, *19*, 20220156. [[CrossRef](#)]
23. Huang, Y.B.; Wu, F. A Sensorless Control Method for Permanent Magnet Synchronous Motor Based on Fractional-Order Sliding Mode Observer. In Proceedings of the 2020 IEEE 5th Information Technology and Mechatronics Engineering Conference (ITOEC 2020), Chongqing, China, 12–14 June 2020; pp. 1536–1542. [[CrossRef](#)]
24. Liu, J.; Li, H.W.; Deng, Y.T. Sliding mode control of permanent magnet synchronous motor based on new approach law and disturbance observer. *J. Eng. Sci.* **2017**, *39*, 933–944. [[CrossRef](#)]
25. Li, Y.; Hu, H.; Shi, P. A Review of Position Sensorless Compound Control for PMSM Drives. *World Electr. Veh. J.* **2023**, *14*, 34. [[CrossRef](#)]
26. Hung, J.Y.; Gao, W.; Hung, J.C. Variable structure control: A survey. *IEEE Trans. Ind. Electron.* **1993**, *40*, 45–55. [[CrossRef](#)]

**Disclaimer/Publisher’s Note:** The statements, opinions and data contained in all publications are solely those of the individual author(s) and contributor(s) and not of MDPI and/or the editor(s). MDPI and/or the editor(s) disclaim responsibility for any injury to people or property resulting from any ideas, methods, instructions or products referred to in the content.